

DOE-ER-40757-112  
 UTEXAS-HEP-98-08  
 MSUHEP-80622  
 MADPH-98-1061

# $\gamma\nu \rightarrow \gamma\gamma\nu$ and crossed processes at energies below $m_W$

Duane A. Dicus

*Center for Particle Physics and Department of Physics  
 University of Texas, Austin, Texas 78712*

Chung Kao

*Department of Physics  
 University of Wisconsin, Madison, Wisconsin 53706*

Wayne W. Repko

*Department of Physics and Astronomy  
 Michigan State University, East Lansing, Michigan 48824  
 (August 4, 2021)*

## Abstract

The cross sections for the processes  $\gamma\nu \rightarrow \gamma\gamma\nu$ ,  $\gamma\gamma \rightarrow \gamma\nu\bar{\nu}$  and  $\nu\bar{\nu} \rightarrow \gamma\gamma\gamma$  are calculated for a range of center of mass energies from below  $m_e$  to considerably above  $m_e$ , but much less than  $m_W$ . This enables us to treat the neutrino-electron coupling as a four-Fermi interaction and results in amplitudes which are electron box diagrams with three real photons and one virtual photon at their vertices. These calculations extend our previous low-energy effective interaction results to higher energies and enable us to determine where the effective theory is reliable.

13.10.+q, 14.60.Gh, 14.80.Am, 95.30.Cq

Typeset using REVTeX

## I. INTRODUCTION

The  $2 \rightarrow 2$  processes  $\gamma\nu \rightarrow \gamma\nu$ ,  $\gamma\gamma \rightarrow \nu\bar{\nu}$  and  $\nu\bar{\nu} \rightarrow \gamma\gamma$ , which have potential astrophysical applications, are known to be highly suppressed due to the vector–axial vector nature of the weak interaction [1–7]. For massless neutrinos, this suppression is such that the cross sections for the  $2 \rightarrow 3$  processes  $\gamma\nu \rightarrow \gamma\gamma\nu$ ,  $\gamma\gamma \rightarrow \nu\bar{\nu}\gamma$  and  $\nu\bar{\nu} \rightarrow \gamma\gamma\gamma$  exceed the  $2 \rightarrow 2$  cross sections for center of mass energies  $2\omega$  between 1 keV and 1 MeV [8]. While this range of energies is adequate for many astrophysical applications, there are those, such as supernova dynamics, where the  $2 \rightarrow 3$  cross sections at higher energies are needed [9]. The low–energy  $2 \rightarrow 3$  cross sections can be calculated from an effective interaction [8], but these results become unreliable for energies on the order of  $m_e$ . Our purpose here is to compute these cross sections using the complete one–loop electron box amplitudes.

In the next Section, we discuss the relation between the low–energy description of  $\gamma\nu \rightarrow \gamma\gamma\nu$  and its crossed channels based on the effective interaction and the more exact numerical treatment of the full amplitude. This is followed by a discussion of the numerical results and their possible applications. The Appendix contains an expression for the photon–photon scattering scalar four–point function in the case when one of the photons is virtual.

## II. $2 \rightarrow 3$ PROCESSES AND VIRTUAL PHOTON–PHOTON SCATTERING

The  $2 \rightarrow 3$  process  $\gamma\nu \rightarrow \gamma\gamma\nu$  and its crossed channels can be calculated using the diagrams illustrated in Fig. 1. When the center of mass energy is small compared to  $m_W$ , the  $W$  and  $Z$  propagators can be replaced by  $m_W^{-2}$  or  $m_Z^{-2}$ . In this case, the diagrams reduce to those for photon–photon scattering with one photon polarization vector replaced by the neutrino current  $\bar{u}(p_2)\gamma_\mu(1+\gamma_5)u(p_1)$  or its crossed channel counterparts. This reduction is illustrated in Fig. 2 for the various channels.

For low–energy scattering, it is possible to describe all  $2 \rightarrow 3$  processes using the effective local interaction [8]

$$\mathcal{L}_{\text{eff}} = 4 \frac{G_F a \alpha^{3/2}}{\sqrt{2}} \frac{1}{\sqrt{4\pi} m_e^4} \left[ \frac{5}{180} (N_{\mu\nu} F_{\mu\nu}) (F_{\lambda\rho} F_{\lambda\rho}) - \frac{14}{180} N_{\mu\nu} F_{\nu\lambda} F_{\lambda\rho} F_{\rho\mu} \right], \quad (1)$$

where  $N_{\mu\nu}$  is

$$N_{\mu\nu} = \partial_\mu (\bar{\psi} \gamma_\nu (1 + \gamma_5) \psi) - \partial_\nu (\bar{\psi} \gamma_\mu (1 + \gamma_5) \psi). \quad (2)$$

Here,  $a = \frac{1}{2} + 2 \sin^2 \theta_W$  includes both the  $W$  and  $Z$  contributions. The dimension 10 operator  $\mathcal{L}_{\text{eff}}$  is closely related to the Euler–Heisenberg Lagrangian for photon–photon scattering [10] and gives the leading term of an expansion in  $\omega/m_e$ . The resulting low–energy cross section,

$$\sigma(2 \rightarrow 3) = \frac{\mathcal{N}(2 \rightarrow 3)}{637 \, 875} \frac{G_F^2 a^2 \alpha^3}{\pi^4} \left( \frac{\omega}{m_e} \right)^8 \omega^2, \quad (3)$$

exhibits a characteristic  $\omega^{10}$  behavior for  $\omega < m_e$ . The numerical factors  $\mathcal{N}(2 \rightarrow 3)$  are

$$\mathcal{N}(\gamma\nu \rightarrow \gamma\gamma\nu) = 1310, \quad (4a)$$

$$\mathcal{N}(\gamma\gamma \rightarrow \nu\bar{\nu}\gamma) = 2144, \quad (4b)$$

$$\mathcal{N}(\nu\bar{\nu} \rightarrow \gamma\gamma\gamma) = 952. \quad (4c)$$

When the center of mass energy exceeds  $2m_e$ , the box diagram develops an imaginary part and it is no longer possible to obtain a reliable estimate of the amplitude by expanding in inverse powers of  $m_e$ . As long as the center of mass energy is small compared to  $m_W$ , it is still possible to calculate the amplitude using the electron box diagrams of Fig. 2 by treating the neutrino current as a virtual photon. For the channels  $\gamma\gamma \rightarrow \nu\bar{\nu}\gamma$  (b) and  $\nu\bar{\nu} \rightarrow \gamma\gamma\gamma$  (c), the virtual photon is timelike, while the virtual photon in the channel  $\gamma\nu \rightarrow \gamma\gamma\nu$  (a) is spacelike. In all cases, the diagrams can be expressed in terms of scalar two-point, three-point, and four-point functions and scalar products of external momenta, photon polarization vectors and the neutrino current [11]. The scalar functions, which are expressible in terms of dilogarithms [12], were evaluated numerically using a FORTRAN code developed for one-loop corrections [13].

### III. DISCUSSION AND CONCLUSIONS

The exact cross sections for all  $2 \rightarrow 3$  channels as a function of the center of mass energy of one of the initial particles are shown in Figs. 3–5, together with the low-energy approximation, Eq. (3). In the  $\gamma\gamma \rightarrow \nu\bar{\nu}\gamma$  and  $\nu\bar{\nu} \rightarrow \gamma\gamma\gamma$  cases, where the virtual photon is timelike, the low-energy result is valid up to energies  $\sim .3 - .4m_e$ . The deviation for a few higher energies is shown in Table I. The ratio of the exact cross section to that given in Eq. (3) becomes unity at  $\omega = 2.1m_e$  and  $1.8m_e$  for the  $\nu\bar{\nu}$  and  $\gamma\gamma$  channels, respectively. Below these crossover points the ratio for these channels is always larger than unity. Consequently, the effective interaction can be used up to these energies to set lower bounds on physical effects.

For the remaining channel,  $\gamma\nu \rightarrow \gamma\gamma\nu$ , where the virtual photon is spacelike, the agreement between the low-energy approximation and the complete calculation is good for energies as large as  $m_e$ . The reason for this difference is related to the behavior of the amplitudes as the center of mass energy of the each initial particle approaches  $m_e$ . For the timelike cases, which, in the context of virtual ( $\gamma^*$ ) photon-photon scattering, correspond to  $\gamma\gamma \rightarrow \gamma\gamma^*$  and  $\gamma^* \rightarrow \gamma\gamma\gamma$ ,  $\omega \rightarrow m_e$  is precisely the threshold for  $e\bar{e}$  production. This is the source of the cusp at  $\omega = m_e$  in Figs. 4 and 5, which is preceded by a departure from the low-energy  $\omega^{10}$  behavior. In the spacelike case ( $\gamma\gamma^* \rightarrow \gamma\gamma$ ), the threshold for  $e\bar{e}$  production requires

$$E'_\nu \leq E_\nu - \frac{m_e^2}{E_\nu}, \quad (5)$$

where  $E_\nu$  is the energy of the initial neutrino and  $E'_\nu$  is the energy of the final neutrino. When  $E_\nu \rightarrow m_e$ ,  $E'_\nu \rightarrow 0$ , and there is essentially no phase space for this. Thus, the development of an imaginary part for  $\gamma\nu \rightarrow \gamma\gamma\nu$  occurs for energies  $E_\nu > m_e$  and the  $\omega^{10}$  behavior persists to a higher value of  $\omega$ . In this case, ratio of the exact cross section to Eq. (3) is less than unity below  $\omega = 1.03m_e$ , grows to 1.71 at  $\omega = 1.30m_e$  and again becomes unity at  $\omega = 1.70m_e$ .

The other feature of Figs. 3–5 is the onset of an  $\omega^2$  behavior once  $\omega \gtrsim 50m_e$ . This is expected since if  $\omega \gg m_e$ , the only scale is  $m_W$  or, equivalently,  $G_F$  and hence the cross section should behave as  $G_F^2\omega^2$ . This behavior, together with the values  $\sigma_{\gamma\gamma \rightarrow \nu\bar{\nu}\gamma} = 5.68 \times 10^{-49} \text{ cm}^2$ ,  $\sigma_{\nu\bar{\nu} \rightarrow \gamma\gamma\gamma} = 4.13 \times 10^{-49} \text{ cm}^2$ , and  $\sigma_{\gamma\nu \rightarrow \gamma\gamma\nu} = 1.74 \times 10^{-48} \text{ cm}^2$  at  $\omega = 100m_e$ , allow accurate extrapolation to all higher energies much less than  $\omega = m_W$ .

As in the low-energy case [8], the final photons in the  $\gamma\nu \rightarrow \gamma\gamma\nu$  channel acquire circular polarization, which is characteristic of a parity violating interaction. The magnitude of this effect is illustrated in Fig. 6, where the difference between the positive and negative helicity cross sections for one of the final photons is plotted relative to the total cross section. There is a reasonably large polarization,  $\sim 20\text{--}30\%$ , for center of mass energies  $< 100 m_e$ .

In addition to the total cross sections, we have investigated the energy and angular distribution of the final neutrino in the process  $\gamma\nu \rightarrow \gamma\gamma\nu$ . The distribution  $d\sigma/dE_\nu$  is shown in Figs. 7 and 8 for a variety of center of mass energies  $\omega$  of the incident photon. In all cases, the distribution of final neutrino energies rises until the inequality Eq. (5) is no longer satisfied, at which point it rapidly drops. The evolution of the angular distribution  $d\sigma/dz$ , where  $z$  is the cosine of the neutrino scattering angle, is shown in Figs. 9 and 10. At  $\omega = m_e$ , the distribution is peaked in the backward direction and this gradually changes into a sharply forward peaked distribution at  $\omega = 100m_e$ .

The processes described here could affect supernovas at several stages of the explosion. Work toward including these reactions in a supernova code is in progress. In addition, the scattering from infrared and optical backgrounds given by these processes could attenuate travel of high energy photons and neutrinos over cosmological distances. The cross sections are too small for significant scattering from cosmic backgrounds.

Finally, it has been noted that the effective interaction, Eq. (1), with one of the photons replaced by an external magnetic field could give enhanced stellar cooling in stars with strong magnetic fields [14]. A more exact calculation, along the lines of this paper, is under consideration.

## ACKNOWLEDGMENTS

We would like to thank V. Teplitz for helpful conversations. This research was supported in part by the U. S. Department of Energy under Grants No. DE-FG02-95ER40896, DE-FG013-93ER40757, in part by the National Science Foundation under Grant No. PHY-93-07780 and in part by the University of Wisconsin Research Committee with funds granted by the Wisconsin Alumni Research Foundation.

## APPENDIX: THE SCALAR FUNCTION $D_0$ FOR $\gamma\gamma \rightarrow \gamma\gamma^*$

The general expression for  $D_0(1, 2, 3, 4)$  with a common internal mass  $m$ , massless external particles  $k_1, k_2, k_3$ , an external particle with  $k_4^2 \neq 0$  and all incoming momenta is [15]

$$D_0(1, 2, 3, 4) = \int_0^1 \frac{dx}{(2k_1 \cdot k_2)(2k_2 \cdot k_3)x(1-x) - m^2(2k_1 \cdot k_3)} \left[ \ln \left( 1 + \frac{2k_1 \cdot k_2}{m^2} x(1-x) - i\varepsilon \right) + \ln \left( 1 + \frac{2k_2 \cdot k_3}{m^2} x(1-x) - i\varepsilon \right) - \ln \left( 1 + \frac{k_4^2}{m^2} x(1-x) - i\varepsilon \right) \right]. \quad (\text{A1})$$

If we introduce the variables  $PX4, PX5$  and  $PX6$  as [11]

$$PX4 = k_4^2 \quad PX5 = (k_1 + k_2)^2 \quad PX6 = (k_2 + k_3)^2,$$

and define  $PX7$  as  $PX7 = PX4 - PX5 - PX6$ , we can write

$$D_0(1, 2, 3, 4) = \int_0^1 \frac{dx}{PX5 PX6 x(1-x) - m^2 PX7} \left[ \ln \left( 1 + \frac{PX5}{m^2} x(1-x) - i\varepsilon \right) + \ln \left( 1 + \frac{PX6}{m^2} x(1-x) - i\varepsilon \right) - \ln \left( 1 + \frac{PX4}{m^2} x(1-x) - i\varepsilon \right) \right]. \quad (A2)$$

In this form, it is clear that, barring cancelations,  $D_0(1, 2, 3, 4)$  has an imaginary part whenever one or more of the  $PXi$ 's satisfies  $PXi < -4m^2$ ,  $i = 4, 5, 6$ .

For the standard decomposition, we define the roots of the polynomials in the logarithms as

$$\beta_{\pm} - i\varepsilon_5 = \frac{1}{2} \left( 1 \pm \sqrt{1 + 4m^2/PX5} \right) - i \frac{|PX5|}{PX5} \varepsilon, \quad (A3)$$

$$\gamma_{\pm} - i\varepsilon_6 = \frac{1}{2} \left( 1 \pm \sqrt{1 + 4m^2/PX6} \right) - i \frac{|PX6|}{PX6} \varepsilon, \quad (A4)$$

$$\delta_{\pm} - i\varepsilon_4 = \frac{1}{2} \left( 1 \pm \sqrt{1 + 4m^2/PX4} \right) - i \frac{|PX4|}{PX4} \varepsilon, \quad (A5)$$

and the roots of the denominator as

$$\lambda_{\pm} = \frac{1}{2} \left( 1 \pm \sqrt{1 - 4m^2 PX7/PX5 PX6} \right). \quad (A6)$$

In terms of these roots, we have

$$\begin{aligned} D_0(1, 2, 3, 4) = & \frac{-1}{PX5 PX6 (\lambda_+ - \lambda_-)} \left\{ -\text{Li}_2 \left( \frac{1 - \lambda_+}{\beta_+ - \lambda_+ - i\varepsilon_5} \right) + \text{Li}_2 \left( \frac{-\lambda_+}{\beta_+ - \lambda_+ - i\varepsilon_5} \right) \right. \\ & - \text{Li}_2 \left( \frac{1 - \lambda_+}{\beta_- - \lambda_+ + i\varepsilon_5} \right) + \text{Li}_2 \left( \frac{-\lambda_+}{\beta_- - \lambda_+ + i\varepsilon_5} \right) - \text{Li}_2 \left( \frac{1 - \lambda_+}{\gamma_+ - \lambda_+ - i\varepsilon_6} \right) \\ & + \text{Li}_2 \left( \frac{-\lambda_+}{\gamma_+ - \lambda_+ - i\varepsilon_6} \right) - \text{Li}_2 \left( \frac{1 - \lambda_+}{\gamma_- - \lambda_+ + i\varepsilon_6} \right) + \text{Li}_2 \left( \frac{-\lambda_+}{\gamma_- - \lambda_+ + i\varepsilon_6} \right) \\ & + \text{Li}_2 \left( \frac{1 - \lambda_+}{\delta_+ - \lambda_+ - i\varepsilon_4} \right) - \text{Li}_2 \left( \frac{-\lambda_+}{\delta_+ - \lambda_+ - i\varepsilon_4} \right) + \text{Li}_2 \left( \frac{1 - \lambda_+}{\delta_- - \lambda_+ + i\varepsilon_4} \right) \\ & - \text{Li}_2 \left( \frac{-\lambda_+}{\delta_- - \lambda_+ + i\varepsilon_4} \right) + \ln \left( \frac{1 - \lambda_+}{-\lambda_+} \right) \left[ \ln \left( -\frac{|PX5|}{PX5} \frac{(PX4 - PX5)}{PX6} + i\varepsilon_5 \right) \right. \\ & - i\pi\theta(PX5) + \ln \left( -\frac{|PX6|}{PX6} \frac{(PX4 - PX6)}{PX5} + i\varepsilon_6 \right) - i\pi\theta(PX6) \\ & - \ln \left( -\frac{|PX4|}{PX4} \frac{(PX4 - PX6)}{PX5} \frac{(PX4 - PX5)}{PX6} + i\varepsilon_4 \right) + i\pi\theta(PX4) \left. \right] \\ & \left. - (\lambda_+ \rightarrow \lambda_-) \right\}, \quad (A7) \end{aligned}$$

where the dilogarithm, or Spence function  $\text{Li}_2(z)$  is defined as

$$\text{Li}_2(z) = - \int_0^1 \frac{dt}{t} \ln(1 - zt) . \quad (\text{A8})$$

For numerical evaluation,  $\text{Li}_2(z)$  can be expanded in powers of  $-\ln(1 - z)$  [12]. The contribution of the logarithms in the square bracket of Eq. (A7) is, at most, a phase.

## REFERENCES

- [1] M. Gell-Mann, Phys. Rev. Lett. **6**, 70 (1961).
- [2] C. N. Yang, Phys. Rev. **77**, 242 (1950); L. D. Landau, Sov. Phys. Doklady **60**, 207 (1948).
- [3] M. J. Levine, Nuovo Cimento **48A**, 67 (1967).
- [4] L. F. Landovitz and W. M. Schreiber, Nuovo Cimento **2A**, 359 (1971).
- [5] V. K. Cung and M. Yoshimura, Nuovo Cimento **29A**, 557 (1975).
- [6] J. Liu, Phys. Rev. D **44**, 2879 (1991).
- [7] D. A. Dicus and W. W. Repko, Phys. Rev. D **48**, 5106 (1993).
- [8] D. A. Dicus and W. W. Repko, Phys. Rev. Lett. **79**, 569 (1997). The channel  $\gamma\gamma \rightarrow \nu\bar{\nu}\gamma$  is discussed in: N. Van Hieu and E. P. Shabalin, Sov. Phys. JETP **17**, 681 (1963).
- [9] M. Harris, J. Wang and V. Teplitz, astro-ph/9707113 (unpublished).
- [10] H. Euler, Ann. Phys. **26**, 398 (1936); W. Heisenberg and H. Euler, Zeit. Phys. **98**, 714 (1936). The connection between these papers and Eq. (1) can be seen by noting that the Hamiltonian is  $\mathcal{H} = -j \cdot A - \ell \cdot W - \ell^\dagger \cdot W^\dagger$ , where  $\ell_\mu$  is the lepton weak current. The the amplitude for pentagon diagram of Fig. 1 involves the time ordered product  $T\{\ell(x_1) \cdot W(x_2) \ell^\dagger(x_2) \cdot W^\dagger(x_2) j(x_3) \cdot A(x_3) j(x_4) \cdot A(x_4) j(x_5) \cdot A(x_5)\}$  together with a combinatorial factor of 20. Contracting the  $W$  fields using the large mass limit of the  $W$  propagator and Fierz rearranging the weak currents gives 4 times the usual expression for the photon-photon scattering amplitude with one photon field replaced by the neutrino current. In addition, there is a term with one axial vector current, which vanishes by Furry's theorem. Eq. (1) then follows. For another discussion see: A. Abada, J. Matias and R. Pittau, hep-ph/9806383 (1998).
- [11] G. Passarino and M. Veltman, Nucl. Phys. **B160**, 151 (1979).
- [12] G. 't Hooft and M. Veltman, Nucl. Phys. **B153**, 365 (1979).
- [13] C. Kao and D. A. Dicus, LOOP, a FORTRAN program for evaluating loop integrals based on the results in Refs. [11] and [12].
- [14] R. Shaisultanov, Phys. Rev. Lett. **80**, 1586 (1998).
- [15] An expression for  $D_0$  in the case when  $k_4$  is timelike is contained in E. W. N. Glover and A. G. Martin, Z. Phys. **C60**, 175 (1993).

# TABLES

$\omega/m_e$	$\nu\bar{\nu}$	$\gamma\gamma$	$\gamma\nu$
0.4	1.38	1.15	0.916
0.5	1.68	1.27	0.883
0.6	2.20	1.49	0.850
0.7	3.17	1.79	0.823
0.8	5.31	2.41	0.809
0.9	11.9	3.95	0.815
1.0	176.	23.3	0.877

TABLE I. The ratio of the exact cross section to that given by Eq. (3) for the various initial particles in the  $2 \rightarrow 3$  reactions is shown.



# FIGURES

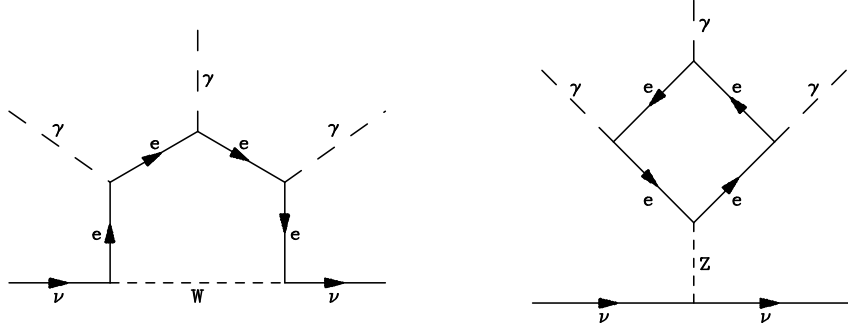


FIG. 1. Typical diagrams for the process  $\gamma\nu \rightarrow \gamma\gamma\nu$  arising from  $W$  (left) and  $Z$  (right) exchange are shown. The complete set is obtained by permuting the photons.

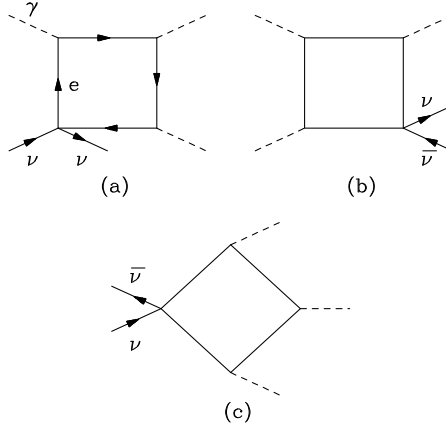


FIG. 2. Typical box diagrams obtained in the limit of large  $m_W$  are shown.

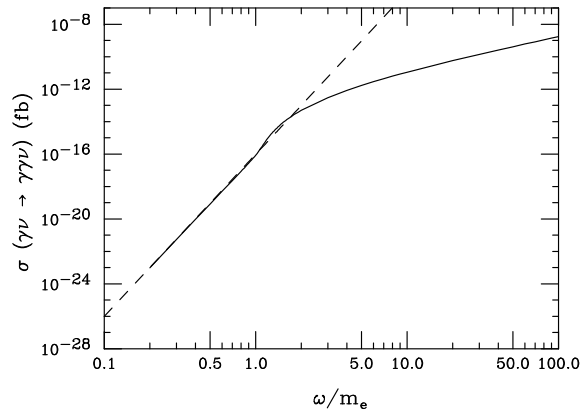


FIG. 3. The cross section  $\sigma(\gamma\nu \rightarrow \gamma\gamma\nu)$  shown as the solid line. The dashed line is the low-energy cross section.

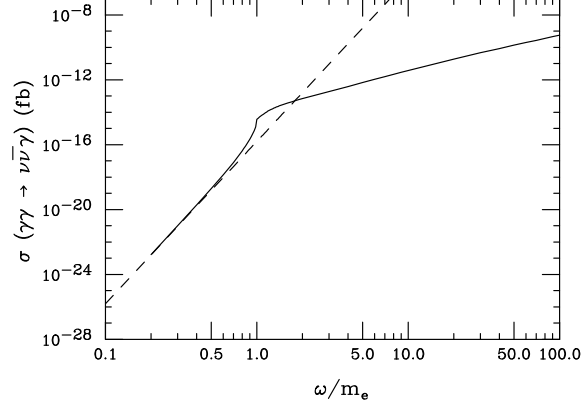


FIG. 4. The cross section  $\sigma(\gamma\gamma \rightarrow \nu\bar{\nu}\gamma)$  shown as the solid line. The dashed line is the low-energy cross section.

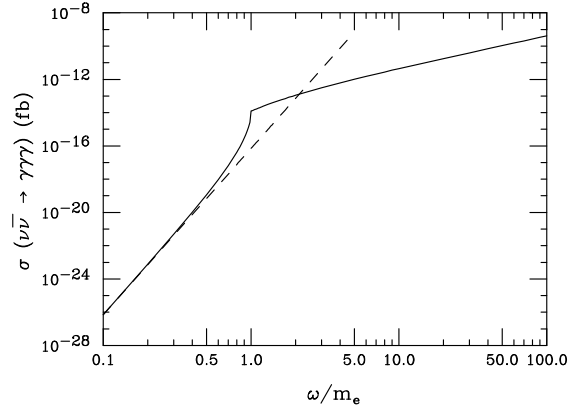


FIG. 5. The cross section  $\sigma(\nu\bar{\nu} \rightarrow \gamma\gamma\gamma)$  shown as the solid line. The dashed line is the low-energy cross section.

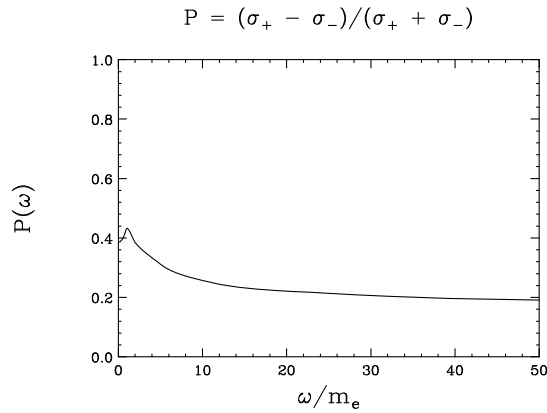


FIG. 6. The circular polarization of one of the final photons in the process  $\gamma\nu \rightarrow \gamma\gamma\nu$  is shown.

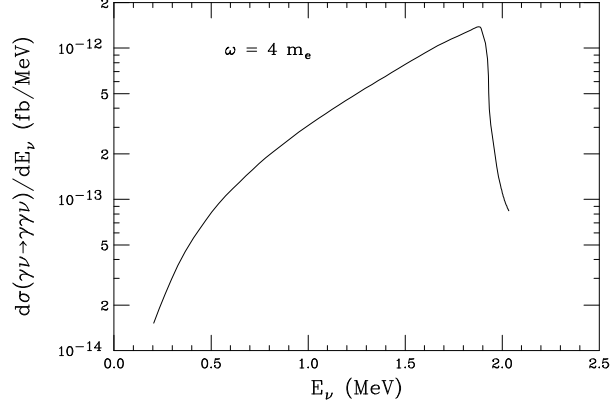


FIG. 7. The distribution of final neutrino energies  $d\sigma/dE_\nu$  is shown for a photon center of mass energy  $\omega = 4m_e$ .

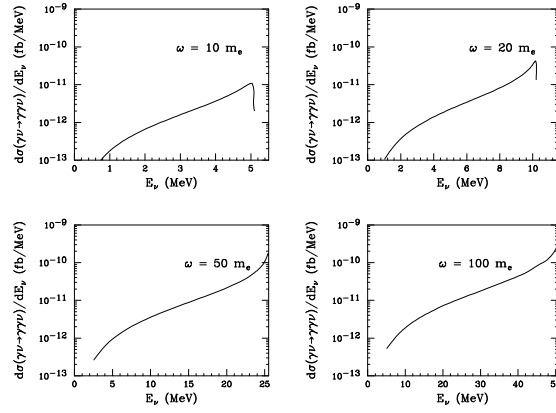


FIG. 8. Same as Fig. 7 for several values of photon center of mass energy  $\omega$ .

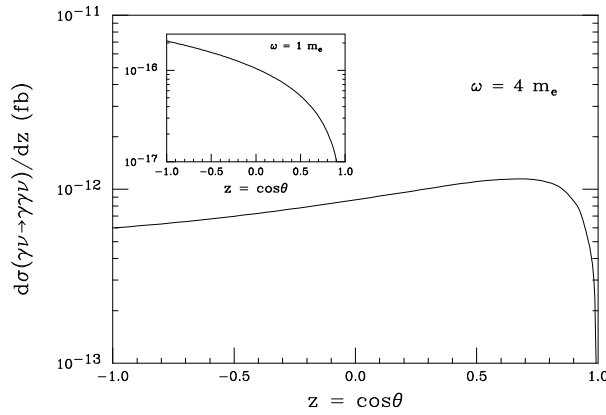


FIG. 9. The angular distribution  $d\sigma/dz$  is shown for  $\omega = 4m_e$ . The inset is the threshold ( $\omega = m_e$ ) distribution, which is very nearly  $(1 - z)$ .

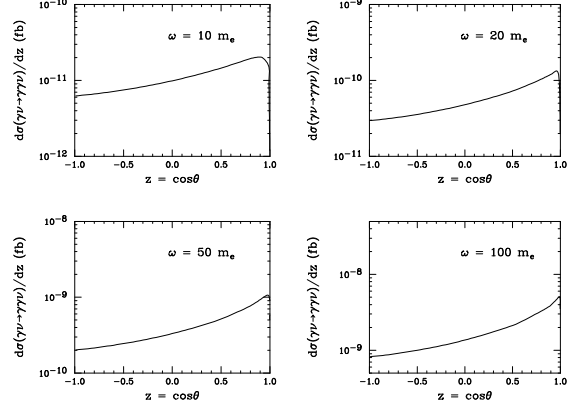


FIG. 10. The angular distribution  $d\sigma/dz$  is shown for several values of  $\omega$ .